NMR Determination of the Magnetic Susceptibility Anisotropy of Cytochrome *c′* of *Rhodobacter Capsulatus* by $^1J_{HN}$ Dipolar Coupling Constants Measurement: Characterization of Its Monomeric State in Solution

Hélène Déméné,† Pascale Tsan, Pierre Gans, and Dominique Marion*

Laboratoire de Résonance Magnétique Nucléaire, Institut de Biologie Structurale "Jean Pierre Ebel" (CEA-CNRS), 41 Rue Jules Horowitz, 38027 Grenoble Cedex, France

Received: December 9, 1999

$^1J_{NH}$ splittings have been measured at 600 and 400 MHz on the paramagnetic ($S = 2$ and $S = {}^5/_2$) and on the diamagnetic state ($S = 0$) of cytochrome *c′* of *Rhodobacter capsulatus*. Residual dipolar splittings and the magnetic susceptibility tensor have been then derived using two methods. The first method equaled for a paramagnetic species the dipolar splitting to the difference of the measured $^1J_{NH}$ splittings between the paramagnetic and diamagnetic forms at one field. The second method consisted in deriving the total magnetic tensor of the paramagnetic forms from the splittings at two fields with a post-correction for the diamagnetic contribution. Both methods are shown to produce equivalent results for the determination of the susceptibility magnetic tensor. Comparison with the magnetic tensor obtained with a previous study based on the dipolar shifts leads to the evidence that, unlike most other cytochromes *c′*, *Rb. capsulatus* cytochrome *c′* of strain M1131 is monomeric in solution. This result is discussed in view of the cytochrome *c′* function. Our study confirms that dipolar splittings are a powerful tool for structure determination, providing insight not only into local structural details but also into the global fold of molecules.

Introduction

Because of the presence of Brownian motion, it is generally taken as granted that all orientations of a protein in solution are evenly distributed. However, angular restriction can occur, leading to an incomplete averaging of the dipolar interaction between spins and to the mergence of residual dipolar splittings.[1] Paramagnetic proteins and nucleic acids are typical biomolecules endowed with the capacity of aligning themselves with respect to the magnetic field due to the intrinsically high anisotropies of their magnetic susceptibility tensor.[2,3] Alternately, dissolving an aspherical molecule in a solvent containing particles which are oriented relative to the magnetic field transfers to the solute a small degree of alignment.[4] The measured dipolar splittings depend on the orientations of the corresponding internuclear vectors all relative to the same frame of reference. They thus represent a new class of structural constraints that one could classify as absolute by contrast to classical NMR constraints such as Overhauser effects (NOEs) and ^3J scalar coupling constants which define relative positions of atoms. Inclusion of this new class of constraints in protocols of structure calculation has proven to significantly improve both the local geometry of the resulting structures as defined by the Ramachandran maps and their precision.[5] On the other hand, providing the fact that a crystallographic or NMR structure is available, determination of the residual dipolar splittings can be an alternative way to the study of the magnetism of metal centers in paramagnetic proteins.[2,6] As compared to residual dipolar couplings, dipolar chemical shifts have a similar angular dependence with respect to the magnetic susceptibility tensor on which a $1/r^3$ variation to the paramagnetic center superimposes. Dipolar shifts thus represent also absolute constraints and have been used as such in a large number of structural studies.[7] However, the dependence in $1/r^3$ entails that dipolar shifts constitute a rather localized probe of the environment of the paramagnetic center in terms of structure and of magnetic susceptibility. From this point of view, residual dipolar splittings whose values are linked to the N−H vector's orientations in the frame of the susceptibility tensor constitute a more delocalized probe of magnetism. These effects were studied on a model system, cytochrome *c′* from *Rhodobacter capsulatus*.

The cytochrome *c′* comprises a unique class of hemoproteins which is found among a wide variety of bacteria with different metabolic pathways ranging from photosynthetic activities (*Chromatiaceae* and *Rhodospirillaceae*), or anaerobic (*Alcaligenes*) to halotolerant (*Parococcus*).[8] Such a variety impairs the clear identification of its biological role. Nevertheless, it has been hypothesized that cytochromes *c′* are implicated in the photosynthetic electron transfer[9,10] as well as in the cellular nitrogen cycle.[10−12] They are class II cytochromes *c*, characterized by heme attachment to the C-terminal region of the protein, a histidine as axial ligand, the absence of a second axial ligand and a low redox potential varying from −10 to 150 mV.[10,12,13] The magnetic properties of ferricytochrome *c′* have been thoroughly investigated with a variety of spectroscopic methods as this oxidized state presents unusual EPR properties.[14] These properties have been described as originating from a quantum admixture of spin state $S = {}^5/_2$ and spin state $S = {}^3/_2$ whose respective proportions depend on the bacteria. The spin state $S = {}^5/_2$ is found to be predominant, *Chromatium vinosum* excepted. The reduced (or ferrous) state has been studied to a less extent but this state presents also unusual NMR paramagnetic spectra.[15] Mössbauer spectroscopy[16] as well as magnetic susceptibility measurements at room temperature[17] have shown

* Corresponding author.
† Present address: Centre de Biochimie Structurale, 15 avenue Charles Flahault, 34060 Montpellier Cedex 2, France.

10.1021/jp994318t CCC: $19.00
Published on Web 02/24/2000

that the reduced state is in a high spin state $S = 2$. EPR studies were unable to detect the typical signal of the ferric state in vivo, and the reduced state is thus probably the physiological one.[18] The heme Fe atom is also able to coordinate CO as a sixth ligand and the reduced protein is then diamagnetic ($S = 0$). Tsan et al. have recently reported a study of the magnetism of the paramagnetic states of cytochrome *c′* of *Rb. capsulatus* (*R.C.* Cyt).[19,20] Determination of the magnetic susceptibility tensor based on the HC^{α}, HN, and ^{15}N dipolar shifts indicate an axial symmetry for spin state $S = {}^5/_2$, with the principal axis perpendicular to the heme plane, whereas surprisingly the tensor is fully asymmetric for spin state $S = 2$ with the principal axis tilted away from the normal to the heme plane.[19,20]

In this paper, we report a study of the magnetic susceptibility tensor of *R.C.* Cyt based on $^1J_{HN}$ dipolar splittings. We have determined the orientation and values of the principal components of the susceptibility tensor for the different magnetic states. Comparison with the tensors derived from the dipolar shifts allows to determine the *R.C.* Cyt oligomerization state in solution. The results are discussed in view of the function of cytochrome *c′*.

Material and Methods

NMR Experiments. All NMR experiments were carried out at 27 °C on ^{15}N-labeled *R.C.* Cyt samples prepared as previously described.[21] Experiments were carried out on Bruker AMX-600 and AMX 400 NMR spectrometers. $^1J_{NH}$ splittings were measured using constant time $^1J_{NH}$-modulated spectra. The scheme was adapted from the one originally proposed by Tjandra and Bax[22] for measuring $^1H-^{13}C$ splittings. Elimination of the water signal is achieved by a WATERGATE sequence (final INEPT transfer) and a selective water flip-back pulse (initial INEPT transfer). A pair of gradients was inserted during the constant time period to ensure proper selection of coherences. Modulation delays Δ of successively 1.9, 2.5, 3.1, 3.7, 5.3, 5.9, 6.5, and 7.1 ms were used. These delays include the duration of the pair of gradients but not of the ^{15}N pulse duration, which must be taken into account when calculating the $^1J_{NH}$ splittings. ^{15}N 90° pulse durations used were 32μs and 20μs at 600 and 400 MHz, respectively. The constant time period T was chosen to be 23.2 and 33.8 ms at 600 and 400 MHz, respectively. On one hand, such durations ensure that a sufficiently large number of t1 points are collected along the indirect dimension at both fields. On the other hand, the first and final modulation delays correspond roughly to the maximum intensity of the sinusoidal signal, to achieve the best experimental precision of the splittings.[23] Time domain data were apodized with a Gaussian (t2) and shifted square cosine (t1) function and zero filled prior to 2D Fourier transformation to yield a digital resolution of 2.34 Hz (t2) and 1.47 Hz (t1) at 600 MHz and of 1.56 Hz (t2) and 0.99 Hz (t1) at 400 MHz, respectively. Spectra were processed with the Felix package (MSI Inc., San Diego).

Extraction of the $^1J_{HN}$ Splittings. The intensity of a $^{15}N-^1H$ correlation peak in the $^1J_{NH}$-modulated spectra should theoretically follow the relation:[22]

$$I = I_0 \cos(2\pi J_{NH}(T + (2/\pi)\tau_{90_N} - \Delta)) \qquad (1)$$

where τ_{90_N} is the length of the 90° pulse on ^{15}N atoms.

In practice, the experimental profile of the intensities was not symmetric with respect to the zero baseline (see Figure 1a) and two possible origins can be considered.

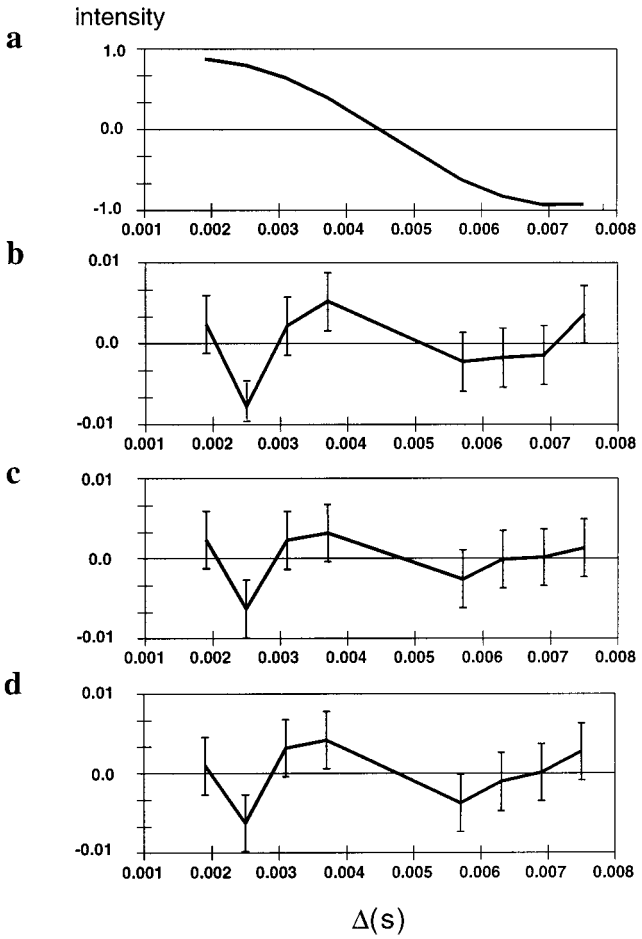

Figure 1. Figure 1: (a) Experimental profile of the intensity I of the N−H correlation peak of residue 4 of *R.C.* Cyt ($S = {}^5/_2$) at 600 MHz as a function of the Δ delay. Experimental points are shown in open boxes. Differences between the experimental intensities of the N−H correlation peak of residue 4 and their best fits according to equation: $I = I_0 \cos(2\pi J_{NH}(T + (2/\pi)90°_{^{15}N} - \Delta)) + I_1$ (b), $I = I_0 \cos(2\pi_{NH}(T + (2/\pi)90°_{^{15}N} - \Delta))\cos(2\pi J_{NH\beta}(T + (2/\pi)90°_{^{15}N} - \Delta))$ (c), $I = I_0 \cos(2\pi_{NH}(T + (2/\pi)90°_{^{15}N} - \Delta))(\exp(2\Delta\sigma_{CSA-DD}) + a\exp(-2\Delta\sigma_{CSA-DD}))$ (d), where J_{NHb} refers to the ^3J coupling constant between the ^{15}N atom and the Hβ atom of the residue and σ_{DD-CSA} to the cross-correlation rate between the dipolar relaxation and CSA relaxation of the ^{15}N atom. Spectral noise is represented as vertical bar. Best fits give $J_{NH} = -93.77$ Hz in (a) ($Chi^2 = 8.3$); -93.42 Hz ($Chi^2 = 5.30$) in (b), and -93.40 Hz ($Chi^2 = 7.0$) in (c).

First, for ^{15}N-labeled proteins, coherence pathway originating from cross-correlation between dipolar relaxation of the N−H vector and the chemical shift anisotropy (CSA) relaxation of the ^{15}N atom takes place. In addition to a direct contribution to the measured $^1J_{NH}$ by the dynamic frequency shift[23] (see the Results and Discussion section), dipolar-CSA cross-correlated relaxation creates magnetization preserving the phase of the original coherence (IxSz → Ix). In the $^1J_{NH}$-modulated HSQC experiment, most of this created magnetization should not be detected, and any residual magnetization gives rise to a dispersive component not interfering with the measurements of intensities.[22,24] However, our theoretical as well as numerical simulations of the evolution of system during the constant time period showed that dipolar-CSA cross-correlation affects also the original ^{15}N antiphase coherence which is to be detected. The final signal is modulated by the factor

$$\exp(2\sigma(\Delta - t_1)) + \exp(2\sigma(t_1 - \Delta))$$

where σ is the dipolar-CSA cross-correlation rate and t_1 is the

incrementable delay of the detection period in the indirect dimension. This modulation can distort the major signal (see simulation in Figure 1d) and induce the lack of symmetry of the experimental signal with respect to zero.

A second phenomenon is due to the indirect ^3J coupling of the ^{15}N atom with the Hβ atom. This leads to an additional factor of $\cos(2\pi\ ^3J_{NH\beta}(T + (2/\pi)\tau_{90_N} - \Delta))$ which modulates the final signal and can also explain the experimental profile detected (see Figure 1c). Simulations show that the bias induced by the $^3J_{NH\beta}$ modulation for $^3J_{NH\beta}$ in the 4−6 Hz range induces a shift ±0.05 Hz for a $^1J_{HN}$ splitting in the 92−96 Hz range (data not shown). However, $^3J_{NH\beta}$ coupling constants are not expected to change between the three states of *R.C.* Cyt for the residues considered. The major part of bias is thus self-eliminated when taking the $^1J_{NH}$ differences.

The quality of the different best-fits to the experimental data could not discriminate between these two coherence pathways; besides, summation over these contributions could be non negligible. Consequently instead of using analytical models, these considerations dictated us the use of the model-independent eq 2 including an additional offset I_1.

$$I = I_0 \cos(2\pi J_{NH}(T + (2/\pi)\tau_{90_N} - \Delta)) + I_1 \qquad (2)$$

The splittings were extracted by means of a simulated annealing program minimizing the error function:

$$E = \sum_n (I_{n,calc} - I_{n,exp})^2/{\sigma_{noise}}^2$$

where n stands for the nth experiment.

The offset in eq 2 accounted for approximately 5% of I_0. Its opposite sign to I_0 revealed to be constant for all residues, indicating that a slight systematic error was indeed taking place. The relative sign and weight of I_1 with respect to I_0 were independent of the magnetic state of the protein. Estimates for random errors in the calculated J_{NH} splittings were extracted from a set of 500 Monte Carlo simulations based on the root-mean-square baseplane noise σ_{noise} in the J-modulated ^{15}N HSQC spectra.

Derivation of the Paramagnetic Susceptibility Tensor. The magnetic susceptibility tensor χ is related to the residual dipolar splittings by

$$J_{NH}^{dip} = f(\chi,B) \qquad (3)$$

where

$$f(\chi,B) = -B^2/(15kT)[\gamma_N\gamma_H/(4\pi^2 {r_{NH}}^3)][\Delta\chi_{ax}(3\cos^2\theta - 1) + {}^3/_2\Delta\chi_{rh}\sin^2\theta\cos(2\phi)]$$

and B is the static magnetic field, $\Delta\chi_{ax}$ and $\Delta\chi_{rh}$ are the axial and rhombic anisotropies of the magnetic susceptibility tensor, and r_{NH}, θ, and ϕ are cylindrical coordinates describing the orientation of the N−H bond vector in the principal axis system of the magnetic susceptibility tensor.

The magnetic susceptibility tensor was derived from the measured $^1J_{NH}$ splittings by two methods.

In the first method, later referred as one-field measurement, the residual dipolar splitting for a paramagnetic form is derived from the values on this form and on the diamagnetic form *at the same field B*:

$$J_{NH}^{dip} = f(\chi,B) = J_p(B) - J_d(B) \qquad (4)$$

The magnetic tensor is then derived by minimizing the error funtion:

$$Chi^2 = \sum_i (J_{i,p}(B) - J_{i,d}(B) - f_i(\chi,B))^2/({\sigma_{i,p}}^2 + {\sigma_{i,d}}^2) \quad (5)$$

where B stands for the spectrometer static field (14.1 or 9.1 T), i is the number of residues taken into account, the subscripts p and d refer to the paramagnetic and diamagnetic form respectively, and σ is the estimated random error. (To avoid confusion with the magnetic susceptibility tensor χ, the error function classically named χ^2 will be referred as Chi^2 in the following.)- This was done successively at 600 and 400 MHz for the paramagnetic forms $S = 2$ and $S = {}^5/_2$.

The second method or two-field measurement consisted in deriving the χ tensor from the difference between the measured $^1J_{NH}$ splittings at 600 and 400 MHz for the same form of *R.C.* Cyt by minimizing the Chi^2 function:

$$Chi^2 = \sum_i (J_{i,p}(600\ MHz) - J_{i,p}(400\ MHz) - (f_i(\chi,600\ MHz) - f_i(\chi,400MHz)))^2/({\sigma_{i,600MHz}}^2 + {\sigma_{i,400MHz}}^2) \qquad (6)$$

Coordinates for the N−H vectors were taken from the X-ray structure.[25] For easier calculations, an Euler rotation of angles $(\alpha,\beta,\gamma) = (0.22, 179.3, 90.22)$ was performed to replace the molecule in the protein inertia frame, the crystallographic frame being the inertia frame of the protein with the crystallization water molecules. The axis z, being a symmetry axis of the molecule, remained unchanged. The rotation was done to assert that the calculations were performed in the symmetry frame of the dimeric molecule.

The magnetic susceptibility tensor was extracted assuming various mathematical models. Model 1 assumes that the χ tensor is axially symmetric and defined by its axial anisotropy $\Delta\chi_{ax}$ and the Euler angles α and β referencing the position of the principal axis. Model 2 assumes a fully anisotropic χ tensor defined by its axial and rhombic anisotropies $\Delta\chi_{ax}$ and $\Delta\chi_{rh}$, and the three Euler angles α, β, and γ positioning the frame of the tensor eigenvectors. In the anisotropic model, the axial and rhombic anisotropies $\Delta\chi_{ax}$ and $\Delta\chi_{rh}$, are related to the eigenvalues χ_1, χ_2, and χ_3 of the magnetic susceptibility tensor by

$$\Delta\chi_{ax} = \chi_3 - (\chi_2 + \chi_1)/2$$

$$\Delta\chi_{rh} = \chi_2 - \chi_1$$

Permutations of the eigenvalues lead to three fundamental different minima (not considering inversion of sign of $\Delta\chi_{rh}$) with the same score Chi^2 which represent the same physical minimum. To alleviate this underdetermination, we used the convention $|\Delta\chi_{ax}| \geq \Delta\chi_{rh} \geq 0$.

All the Chi^2 minimizations were performed using a simulated annealing algorithm developed in our laboratory.[26] The errors in the extracted parameters and the validation of each model were derived using 250 Monte Carlo simulations. Models were accepted if they could give rise to the measured dipolar splittings within 95% confidence limits. If both model 1 (axial) and model 2 (anisotropic) were simultaneously accepted, the statistical significance of the decrease in the Chi^2 function brought by two additional degrees of freedom was tested by using a F-test based on Monte Carlo simulations.[26] Sets of Gaussian distributions of dipolar splittings centered on the dipolar splittings back-calculated with the axial tensor minima were generated. These

simulated data were simultaneously fitted with an axial and an anisotropic model and the ratio $p = (Chi_{ax}^2 - Chi_{anis}^2)/Chi_{anis}^2$ calculated. If the factor p_{exp} calculated with the Chi^2 values from the fit of the real experimental data with the axial and anisotropic models was found to lie in the 20% highest simulated p ratios, the use of an anisotropic model was considered to be statistically significant versus the axial model.[26]

Correction for the Diamagnetic Contribution in the Two-Field and One-Field Methods. Using the two-field measurement method, the sum tensor $\chi_{sum} = \chi_p + \chi_d$ is experimentally determined, and eq 7 is used, as previously described,[6] to calculate the true magnetic tensor χ_p.

$$\chi_p = \chi_{sum} - \chi_d \tag{7}$$

In this case, the diamagnetic tensor should be either computed or experimentally determined (cf. next section). Use of the two-field measurement method assumes that the magnetic tensor is independent from the magnetic field. According to the Brillouin equation,[27] this assumption holds true for the range of magnetic fields used in this study (9−14 T).

Deriving the magnetic tensor with the one-field measurement method supposes that the contribution to the dipolar splitting of the diamagnetic tensor is identical between the paramagnetic and diamagnetic states. If the diamagnetic and the paramagnetic susceptibility tensors are collinear, then the measured residual coupling is merely the sum of the diamagnetic and paramagnetic contribution. If the tensors are not collinear, the situation is more complex: the experimental splitting can be decomposed for the paramagnetic state as

$$J_p(B) = J^{scal} + J^{dip}(\chi_{sum},\alpha_{sum},\beta_{sum},\gamma_{sum},B)$$

and for the diamagnetic one as

$$J_d(B) = J^{scal} + J^{dip}(\chi_d,\alpha_d,\beta_d,\gamma_d,B)$$

J^{scal} is the scalar one-bond coupling constant; the orientation of the sum tensor $\chi_{sum} = \chi_p + \chi_d$ is given by the Euler angles $(\alpha_{sum},\beta_{sum},\gamma_{sum})$ and that of the diamagnetic tensor χ_d by the Euler angles $(\alpha_d,\beta_d,\gamma_d)$. The knowledge of χ_d (either theoretical or from experimental data) allows to calculate the diamagnetic dipolar splitting $J_d^{dip}(\chi_d,\alpha_d,\beta_d,\gamma_d,B)$ at a given field B. A more accurate estimate of the susceptibility tensor χ_{sum} of the two paramagnetic states $S = 5/2$ and $S = 2$ can be then derived using the following equation:

$$f(\chi_{sum},B) = J_p(B) - J_d(B) + J_d^{dip}(\chi_d,\alpha_d,\beta_d,\gamma_d,B)$$

The true paramagnetic tensor χ_p is then simply obtained from eq 7.

Diamagnetic Tensor Determination. The diamagnetic contribution to the overall magnetic susceptibility arises in first approximation from the individual diamagnetic susceptibilities of the π-electron bonds: i.e., the porphyrin group, the backbone carbonyl bonds, and the side chains of aromatic residues. It can be calculated theoretically as the sum of these components on the following basis. The magnetic susceptibility anisotropy of the heme and of the aromatic side chains is axially symmetric and oriented perpendicularly to the ring planes, with $\Delta\chi_{ax}$ values of -0.757×10^{-8} m^3/mol (porphyrin),[28] and, for the aromatic side chains,[29] -0.148×10^{-8} (Trp), -0.076×10^{-8} (Phe), -0.071×10^{-8} (Tyr), and -0.041×10^{-8} m^3/mol (His). The magnetic anisotropy of a peptide group can reasonably be assumed to be axially symmetric and perpendicular to its plane with a magnitude of -0.011×10^{-8} m^3/mol.[30] The major contribution to the susceptibility tensor of the protein stems from the porphyrin group and thus possible discrepancies between the solution and crystal structures due to mobility of side chains will have only marginal influence.

Alternately, the diamagnetic tensor can be experimentally derived from the measurements at two fields of the $^1J_{NH}$ splittings of the diamagnetic form using eq 6.

Results and Discussion

$^1J_{NH}$ Residual Dipolar Splittings Determination. For cytochrome $S = 2$, 88 and 91 splittings could be measured from resolved N−H correlation peaks at 600 and 400 MHz, respectively; for cytochrome $S = 5/2$, 72 and 69, and for cytochrome $S = 0$, 113 and 100, respectively (Tables S1−S6, Supporting Information). The $^1J_{NH}$ differences obtained with methods 1 and 2 are shown for the paramagnetic forms $S = 5/2$ in Figure 2a−c and $S = 2$ in Figure 2d−f.

As expected, the largest effect is observed for the differences $(J_p - J_d)$ at 600 MHz. At 400 MHz, this effect is approximatively scaled down by a factor of 2 as expected for a B^2 dependence. The profiles obtained using the one-field or two-field method cannot be compared rightaway, as they reflect different tensors. The most striking feature in comparing the results of both paramagnetic forms is the systematic inversion of sign of the observed effects.

As pointed out in the Material and Methods section, the experimental J-splittings are obtained from the pattern of modulation of the signal intensities. Other phenomena (than residual coupling) could contribute to the apparent $^1J_{NH}$ splitting. We thus have evaluated the impact of three possible phenomena prone to take place during the constant-time evolution of the transverse coherence of the ^{15}N atoms. First, Harbison[31] has shown that the measurement of J-splitting can be biaised due to differential relaxation rates between the in-phase and antiphase ^{15}N coherences: this contribution will be called $^1J_{NHdr}$. Second, dynamic frequency shift due to cross correlation between dipolar and diamagnetic CSA interactions leads to a contribution $^1J_{NHdiaDFS}$ to the apparent splitting $^1J_{NH}$.[23] Last, for the paramagnetic states of *R.C.* Cyt only, dynamic frequency shift ($^1J_{NHparaDFS}$) also occurs due to cross correlation between two dipolar mechanisms: the NH dipole−dipole interaction and the nuclear spin−Curie spin dipolar interaction.[32]

The observed $^1J_{NH}$ splittings are consequently the sum of all these contributions

$$^1J_{NH} = {}^1J_{NHscalar} + {}^1J_{NHdip} + {}^1J_{NHparaDFS} + {}^1J_{NHdiaDFS} + {}^1J_{NHdr}$$

In the one-field method, where the J_{NH}^{dip} is derived from the difference $^1J_{NHpara}(B) - {}^1J_{NHdia}(B)$, the bias introduced arises only from the $^1J_{NHparaDFS}$ contribution. Although this contribution can be of similar magnitude as the observed effects for spins close to the iron (for instance, −1.5 Hz for F14 NH at 6.5 Å from the iron center ($S = 5/2$ at 600 MHz)), all protons considered for the magnetic susceptibility tensor determination are located at more than 10 Å from the iron center (this contribution drops to less than 0.2 Hz and compares with the uncertainty range). In the two-field method, the resulting value of the residual dipolar splitting should be corrected from $({}^1J_{NHparaDFS} + {}^1J_{NHdiaDFS} + {}^1J_{NHdr})_{600} - ({}^1J_{NHparaDFS} + {}^1J_{NHdiaDFS} + {}^1J_{NHdr})_{400}$. The paramagnetic term can be neglected for the same reasons as in the one-field method. Although the $^1J_{NHdiaDFS}$ term are not negligible (respectively −0.51 Hz and −0.46 Hz at 600 and

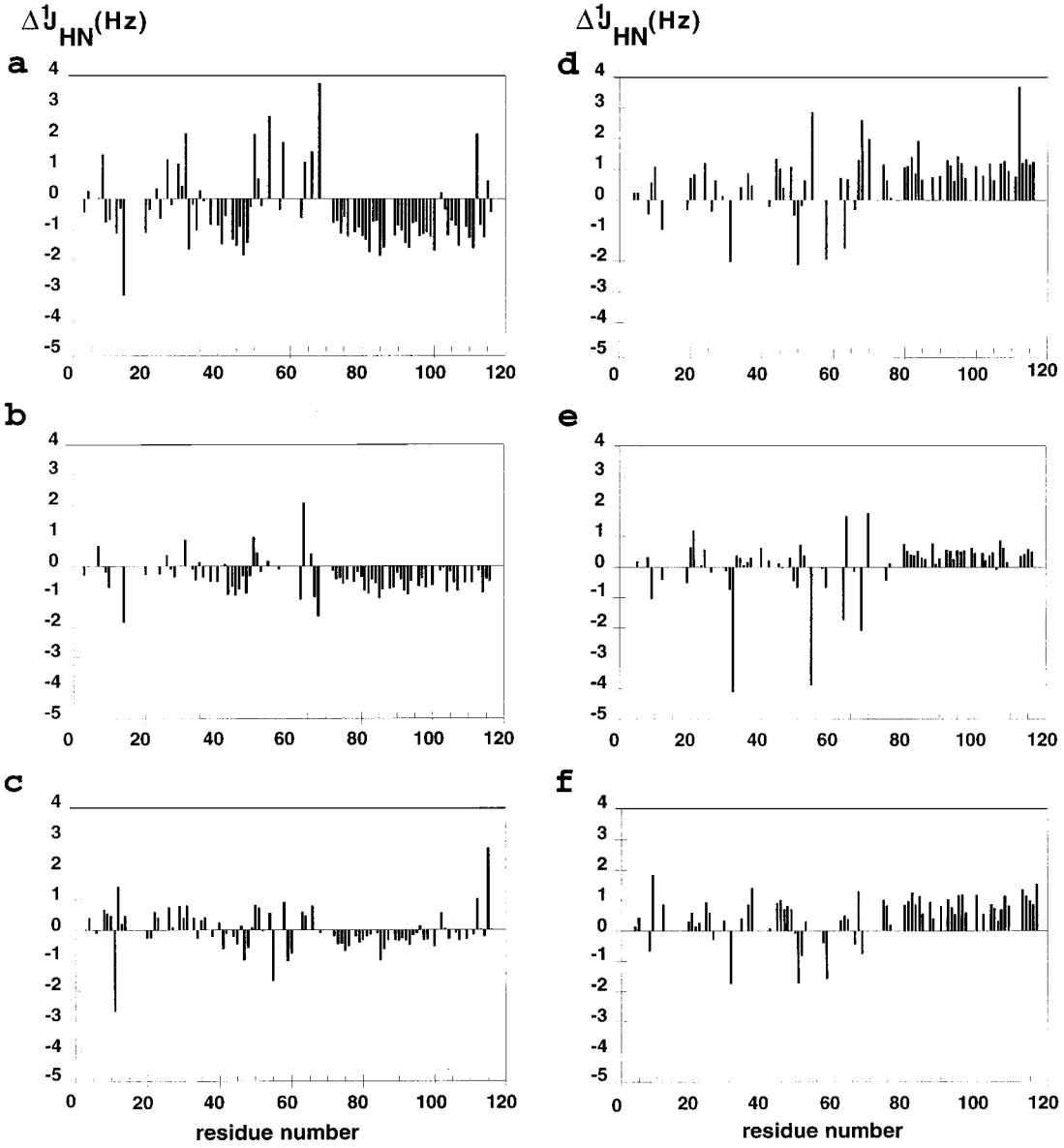

Figure 2. Plot as a function of the residue number in the *R.C.* Cyt sequence of the differences between the measured $^1J_{NH}$ splittings (a) of the paramagnetic form $S = 2$ and of the diamagnetic form $S = 0$ at 600 MHz; (b) of the paramagnetic form $S = 2$ and of the diamagnetic form $S = 0$ at 400 MHz; (c) of the paramagnetic form $S = 2$ at 600 and at 400 MHz; (d) of the paramagnetic form $S = {}^5/_2$ and of the diamagnetic form $S = 0$ at 600 MHz; (e) of the paramagnetic form $S = {}^5/_2$ and of the diamagnetic form $S = 0$ at 400 MHz; (f) of the paramagnetic form $S = {}^5/_2$ at 600 and at 400 MHz. For clarity, the errors bars are not represented, since the mean measured effect is low compared to the maximum errors. The complete data are represented in Figure S1 (in Supporting Information).

400 MHz[33]), only the difference is relevant here, i.e., about 0.05 Hz. For the differential relaxation term $^1J_{NHdr}$, numerical simulations assuming a 10 ns correlation time showed that for $J = -94$ Hz, the induced shift is only of -0.07 Hz at 600 and -0.04 Hz at 400 MHz and that the difference can be safely neglected. Furthermore, one can note that the diamagnetic dynamic shift effect is counterbalanced by the overestimation of the splitting due to the difference in the relaxation rates of in-phase and antiphase coherences.

Derivation of the Magnetic Susceptibility Tensor of the Paramagnetic Forms. Magnetic properties of the different spin states can be assessed using eq 3 by a fit of the magnetic susceptibility magnitude and orientation. For the paramagnetic states, it is, however, necessary to assume that the electron density is localized on the Fe center, a simplification which is only justified for nuclei located at least 10 Å away from the metal center.[34] This criterion is justified for all the nuclei considered in the present discussion. For cytochrome $S = 2$, the fit was performed using 83 splittings (64 whose difference was higher than the corresponding sum of estimated errors) with the one-field method at 600 MHz, 71 (48) at 400 MHz, and 86 (70) with the two-field method. For cytochrome $S = {}^5/_2$, the fit was performed using 65 (55) splittings with the one-field measurement at 600 MHz, 67 (46) at 400 MHz, and 65 (56) with the two-field method.

Data were fitted using either axially symmetric (three parameters) or fully anisotropic models (five parameters) and the results are listed in Table 1 for spin state $S = 2$ (line A) and for spin state $S = {}^5/_2$ (line B).

The susceptibility tensor of the heme Fe is characterized by a high axial anisotropy $\Delta\chi_{ax}$ of comparable amplitude for both forms, but of opposite signs. This corresponds to the inversion of sign in the differences of splittings mentioned above. The spin state $S = 2$ is characterized by a high rhombic anisotropy $\Delta\chi_{rh}$, approximately the third of the axial anisotropy, and the axial model is rejected. The significance of the need for this

TABLE 1: Axially and Anisotropic Magnetic Susceptibility Tensors from $^1J_{NH}$ Splittings for the Reduced and Oxidized States of Cytochrome *c′* of *Rb. Capsulatus*

Best Fit Using the Symmetric Model

	α	β	$\Delta\chi_{ax}$ (10^{-8} m^3/molecule)	Chi_{exp}^2	$Chi_{0,05}^2$
(A) $S = 2$					
1[a]	79.3 ± 0.6	93.1 ± 1.2	2.50 ± 0.05	221.9	102.4
2[b]	75.1 ± 1.3	117.9 ± 2.7	2.70 ± 0.01	151.9	75.1
3[c]	93.0 ± 0.9	88.1 ± 1.9	1.79 ± 0.06	127.8	107.8
(B) $S = 5/2$					
1[a]	75.9 ± 0.9	130.5 ± 1.1	−2.63 ± 0.05	65.8	80.7
2[b]	72.0 ± 2.0	132.4 ± 2.6q	−2.51 ± 0.14	56.7	86.2
3[c]	74.2 ± 1.2	130.0 ± 1.3	−3.82 ± 0.11	78.4	84.0

Best Fit Using the Anisotropic Model

	α	β	γ	$\Delta\chi_{ax}$ (10^{-8} m^3/molecule)	$\Delta\chi_{rh}$ (10^{-8} m^3/molecule)	Chi_{exp}^2	$Chi_{0,05}^2$
(A) $S = 2$							
1[a]	82.5 ± 0.6	102.4 ± 1.8	158.2 ± 1.6	2.56 ± 0.05	0.86 ± 0.07	96.4	98.7
2[b]	78.1 ± 1.3	118.7 ± 3.3	156.3 ± 3.5	2.46 ± 0.17	1.06 ± 0.11	78.5	82.7
3[c]	91.4 ± 1.1	94.2 ± 2.2	131.3 ± 5.1	1.91 ± 0.06	0.60 ± 0.07	73.7	102.6
(B) $S = 5/2$							
1[a]	75.8 ± 0.9	130.7 ± 1.3	189.0 ± 32	−2.72 ± 0.10	0.02 ± 0.11	65.7	75.0
2[b]	73.7 ± 2.2	126.9 ± 4.8	104.1 ± 7.7	−1.93 ± 0.21	0.53 ± 0.01	47.1	80.0
3[c]	74.1 ± 1.3	129.1 ± 2.7	85.1 ± 26	−3.80 ± 0.26	0.26 ± 0.23	73.6	79.5

F Statistics Using Five-Parameter Fitting of Data Simulated from Three-Parameter Model

	$[(Chi_{ax}^2 - Chi_{anis}^2)/2Chi_{anis}^2]_{exp}$	$[(Chi_{ax}^2 - Chi_{anis}^2)/2Chi_{anis}^2]_{0.80}$
(A) $S = 2$	0.6511	0.0178
	0.4683	0.0225
	0.3669	0.0190
(B) $S = 5/2$	0.0007	0.0240
	0.1014	0.0267
	0.0327	0.0388
(C) $S = 0$	0.3483	0.0215

[a] Method 1: χ extracted using the relation: $f(\chi,600\text{ MHz}) = J_p(600\text{ MHz}) - J_d(600\text{ MHz})$. [b] Method 1: χ extracted using the relation: $f(\chi,400\text{ MHz}) = J_p(400\text{ MHz}) - J_d(400\text{ MHz})$. [c] Method 2: χ extracted using the relation: $f(\chi,600\text{ MHz}) - f(\chi,400\text{ MHz}) = J_p(600\text{ MHz}) - J_p(400\text{ MHz})$.

high rhombic anisotropy to fit the experimental data is clearly confirmed by the F-test based on Monte Carlo simulations (Table 1). By contrast, experimental data of the spin state $S = {}^5/_2$ are satisfactorily fitted using only an axial model. Using the fully anisotropic model yields a very weak rhombic anisotropy with high errors in both its value and the location of the corresponding eigenaxes. Correspondingly, statistical significance of the addition of the two supplementary fitted parameters is not achieved for two of the three results (one-field measurement at 600 MHz and two-field measurement at 600 and 400 MHz).

Derivation of the Magnetic Susceptibility Tensor of the Diamagnetic Form: Case of Multiple Minima. The diamagnetic tensor was derived from the splittings measured for spin state $S = 0$ at 400 and 600 MHz using eq 6. For the fit, 108 splittings were used (34 whose difference was higher than the sum of the respective estimated error, see Supporting Information). Although the measured effects are weak, data could be satisfactorily fitted to a susceptibility tensor. Results are summarized in Table 2. The diamagnetic tensor is characterized by a relatively high negative axial anisotropy and a low rhombic component, although nonnegligible (see the F-test statistic in Table 1). Because of the high weight of experimental errors relative to the dipolar splitting measured, estimated errors for the fitted tensor are approximately 3 times higher than for the paramagnetic states of the protein. Interestingly, fitting of the experimental data with the axial model led to two different axial minima almost orthogonal with very close scores, minimum 1 and minimum 2, which were statistically accepted. This prompted us to inspect more closely the energetic surface of the error functions for the previous fits performed for spin state $S = 2$ and $S = {}^5/_2$ using an axial model. We systematically found two perpendicular energetic minima. The angle θ between the principal axes was in the 77°−101° range. However, the diamagnetic state is the sole case where both minima are accepted. Comparing with the results from the anisotropic model, we found that these two axial minima essentially correspond to two of the three equivalent minima of the anisotropic model (values and orientation), with the following rules: if $|\chi_3 - \chi_2| \geq |\chi_3 - \chi_1| \geq \chi_1 - \chi_2 \geq 0$, the two axial minima found are $\Delta\chi_{ax} = \chi_3 - (\chi_2 + \chi_1)/2$ (minimum 1, lower score Chi^2) and $\Delta\chi_{ax} = \chi_2 - (\chi_3 + \chi_1)/2$ (minimum 2, higher score Chi^2), thus with axial anisotropies of opposite signs.[35] Figure 3 depicts the distribution of the two axial minima and of the three equivalent anisotropic minima calculated with the Monte Carlo simulations for the data collected for cytochrome $S = 2$ at 400 MHz. The difference in the score Chi^2 of the two axial minima tends to be as low as the real model tends to be anisotropic and the eigenvalues of the tensor equally spaced. This is illustrated by the case of the diamagnetic case. The presence of two equivalent orthogonal axial minima with opposite signs for the susceptibility tensor of the high-spin ferrous myoglobin derived from a ^{1}H dipolar shift study has been recently reported.[36] It is likely that, as pointed out by the

TABLE 2: Axially and Anisotropic Magnetic Susceptibility Tensors from $^1J_{NH}$ Splittings for the Diamagnetic State of Cytochrome *c′* of *Rb. capsulatus*

Best-Fit Using the Symmetric Model[a]

	α	β	$\Delta\chi_{ax}$ (10^{-8} m^3/molecule)	Chi_{exp}^2	$Chi_{0,05}^2$
$S = 0$					
minimum 1	65.4 ± 2.2	128.7 ± 3.4	−1.18 ± 0.15	124.0	132.5
minimum 2	157.6 ± 3.2	84.8 ± 3.6	0.67 ± 0.04	126.6	129.1

Best-Fit Using the Anisotropic Model

	α	β	γ	$\Delta\chi_{ax}$ (10^{-8} m^3/molecule)	$\Delta\chi_{rh}$ (10^{-8} m^3/molecule)	Chi_{exp}^2	$Chi_{0,05}^2$
$S = 0$	66.0 ± 8.2	120.1 ± 9.3	88.9 ± 22.5	−0.76 ± 0.18	0.40 ± 0.23	106.1	125.6

F Statistics Using Five-Parameter Fitting of Data Simulated from Three-Parameter Model

	$[(Chi_{ax}^2 - Chi_{anis}^2)/2Chi_{anis}^2]_{exp}$	$[(Chi_{ax}^2 - Chi_{anis}^2)/2Chi_{anis}^2]_{0.80}$
$S = 0$		
minimum 1	0.096	0.016
minimum 2	0.084	0.016

[a] Values of χ components were obtained using the two-field measurement method.

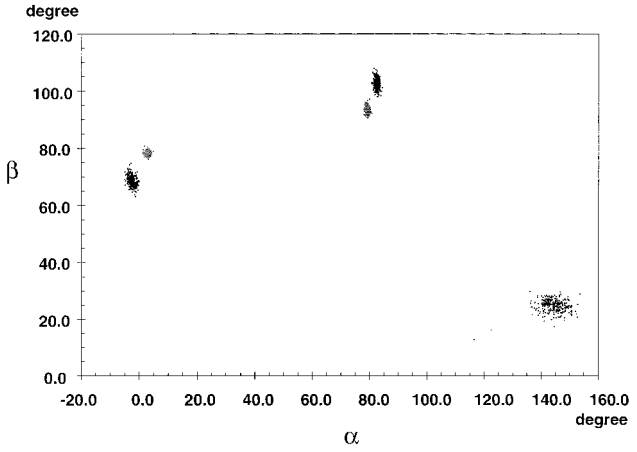

Figure 3. Distribution of the α and β angles referring to the position of the principal axis of the three equivalent minima issued from the Monte Carlo simulations using the anisotropic model (black open triangles) and of the two (nonequivalent) minima using the axially symmetric model (light gray crosses) for *R.C.* Cyt ($S = 2$) at 400 MHz.

authors, this reflects the existence of nonnegligible rhombic magnetic anisotropy in this compound and that the use of a fully anisotropic model would have been justified. The existence of different perpendicular minima using an axial model has been already identified for the determination of the rotational diffusion tensor of a protein from the ratio of the relaxation times R_2/R_1.[26,37] Three minima theoretically coexist, where the axial principal diffusion value globally corresponds to the three eigenvalues and eigenvectors of the diffusion tensor.

Correction for the Orientational NH Bond Fluctuations and Diamagnetic Contribution. Any mobility of the N−H bond within the NMR time scale introduces a bias in the determination of the dipolar splitting value due to the averaging over the N−H vector orientation. Assuming an anisotropic rotational diffusion tensor, ^{15}N relaxation of the carbon monoxide complex of the ferrocytochrome *c′* can be modeled using the formalism of Lipari and Szabo[38] without any chemical exchange.[39] The order parameter S_{fast}^2 is very uniform along the protein sequence with a mean value of 0.880 ± 0.003, indicating a rigid protein. Among the residues taken in account for the $^1J_{NH}$ calculations, only three residues have an internal correlation time greater than 10 ps. One residue has an internal correlation time greater than 100 ps and has been discarded. Consequently, introducing the residue-specific order parameter S_{fast} in eq 3 led to similar results, with the expected scaling of the anisotropies by a factor in the 1/0.90−1/0.95 range (see line $S = 0$ in Table 3). The uncertainties in the order parameters are, however, far too high (of the order of the percent compared to uncertainties of the thousand for the splittings) to allow relevant Monte Carlo simulations to estimate the errors in the derived parameters.

TABLE 3: Magnetic Susceptibility Tensors from $^1J_{NH}$ Splittings Corrected for NH Bond Fluctuations and for the Diamagnetic Contribution for the Different States of Cytochrome *c′* of *Rb. capsulatus*

	α	β	γ	$\Delta\chi_{ax}$ (10^{-8} m^3/molecule)	$\Delta\chi_{rh}$ (10^{-8} m^3/molecule)
(A) $S = 2$					
1[a]	82.4	102.5	158.2	2.39	0.87
2[b]	78.0	118.5	155.1	2.61	1.10
3[c]	83.1	100.7	144.6	2.62	0.76
(B) $S = 5/2$					
1[a]	75.1	130.0	179.1	−2.94	0.07
2[b]	72.6	125.4	183.2	−2.59	0.33
3[c]	76.2	130.7	189.8	−3.04	0.18
(C) $S = 0$					
1[c]	67.5	117.1	81.2	−0.82	0.41

[a] Method 1: χ extracted using the one-field measurement method at 600 MHz. [b] Method 1: χ extracted using the one-field measurement method at 400 MHz. [c] Method 2: χ extracted using the two-field measurement method.

Table 3 lists the susceptibility tensor of the spin state $S = {}^5/_2$ and $S = 2$ corrected for the diamagnetic contribution for the two methods. The corrected results from the fits at one field remain unchanged and lie within the errors of the raw fits, whereas the corrected results for the fit at two fields are significantly different. Although the fitted diamagnetic tensor cannot be fitted precisely, a better agreement is obtained between the results at one field and that at two fields when this tensor is taken into account. Interestingly, although the diamagnetic contribution to the susceptibility tensor is not negligible, as indicated by the large over- and underdetermination for spin state $S = {}^5/_2$ and $S = 2$, respectively, of the absolute value of the axial component determined in the two-field method, the tensor determined from the one-field method without diamagnetic correction is a good approximation of the paramagnetic

TABLE 4: Magnetic Susceptibility Tensors from $^1J_{NH}$ Splittings (J^{dip}), Dipolar Shift Measurements (δ, ppm) and Theoretical Calculations (calc) for Cytochrome *c′* of *Rb. capsulatus*

	α	β	γ	$10^{-8}\Delta\chi_{ax}$ (m^3/mol)	$10^{-8}\Delta\chi_{rh}$ (m^3/mol)
(A) $S = 2$					
J^{dip} [a]	82.4	102.5	158.2	2.39	0.87
δ (ppm)	80.1	109.2	155.1	2.88	0.85
(B) $S = {}^5/_2$					
J^{dip} [a]	75.1	130.0	179.1	−2.94	0.07
δ (ppm)	74.8	135.2	172.1	−2.93	0.02
(C) $S = 0$					
J^{dip} [b]	67.5	117.1	81.2	−0.82	0.41
calc	72.6	132.9	91.0	−0.94	0.29

[a] Method 1: χ extracted using the one-field measurement method at 600 MHz. [b] Method 2: χ extracted using the two-field measurement method.

susceptibility tensor. This holds true even in the $S = 2$ state where the paramagnetic and diamagnetic tensors are not strictly collinear: to a first approximation, the eigenvalues of the resulting tensor can be considered as the sum of the eigenvalues of the two tensors if the rhombic contribution and the underlying angle remain small.

Comparison with the Dipolar Shift Derived Tensors. Tsan et al. used the differences between the chemical shifts in the paramagnetic forms and diamagnetic form of *R.C.* Cyt to derive the susceptibility magnetic anisotropies.[19,20] The dipolar shift obeys the following equation:

$$\delta_{ppm} = (1/3r^3)[\Delta\chi_{ax}(3\cos^2\theta - 1) + {}^3/_2\Delta\chi_{rh}\sin^2\theta\cos(2\phi)]$$

where r is the distance of the considered nucleus and the Fe atom.

Compared to the dipolar splittings, the dipolar shift is also dependent on the r distance between the nucleus and the Fe atom. Thus, according to the crystal structure of *R.C.* Cyt, the dipolar field of the Fe atom of a subunit is negligible for the nuclei of the second subunit. As a result, the tensor derived from the dipolar shift corresponds to a monomer. By contrast, the dipolar splittings are independent of the distance to the Fe atom. Because of the additivity of the magnetic tensors, the tensor characterized in the present study for the dimeric *R.C.* Cyt is thus the addition of the two subunit tensors. Table 4 summarizes the results obtained by the two methods, dipolar shift and dipolar splittings measurements. Surprisingly, the tensors obtained by both methods are very similar in terms of orientations as well as of eigenvalues. The orientations and the magnitude of the eigenvalues of the tensor are vizualized in Figure 4. For the oxidized form ($S = {}^5/_2$), for both methods, the principal axis defining the axial anisotropy is perpendicular to the heme plane whereas for the reduced form ($S = 2$), there is a similar deviation of this axis from the normal to the heme plane. The principal axis of the susceptibility tensor displays an angle (with respect to the heme normal) of 2° and 3.5° (for $S = {}^5/_2$) and 27° and 32° (for $S = 2$) in the dipolar shift study and in this study, respectively. More suprisingly, none of the principal directions of the magnetic susceptibility tensor as calculated with the dipolar splittings coincide with the direction of the symmetry axis of the dimer (the z axis) of the X-ray structure. In that case, the Euler angle β would be equal to 0° or 90° (±180°). If *R.C.* Cyt is actually a dimer, as proposed for several other species, the magnetic susceptibility tensor would have one of its principal axis along the symmetry axis, which is not observed, in particular for the oxidized form. This

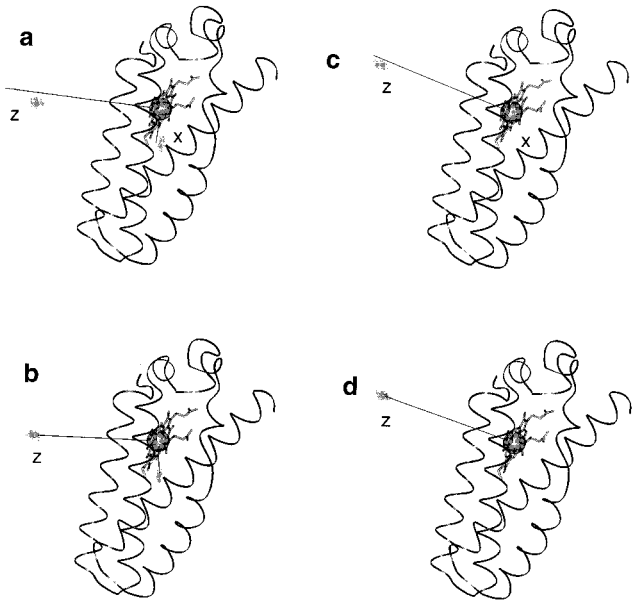

Figure 4. Representation of the orientations for the magnetic susceptibility tensors of *R.C.* Cyt derived (a) for the spin state $S = 2$ from the dipolar chemical shifts; (b) for the spin state $S = 2$ from the dipolar splittings (method 1 at 600 MHz, Table 1); (c) for the spin state $S = {}^5/_2$ from the dipolar chemical shifts; (d) for the spin state $S = {}^5/_2$ from the dipolar splittings (method 1 at 600 MHz, Table 1). The directions of the eigenvectors (x and z) corresponding to the minima determined from the experimental data are represented by straight lines. Their lengths are proportional to the rhombic and axial anisotropies, respectively. For the spin state $S = {}^5/_2$, only the z component is represented, as rhombicity was shown to be negligible. The spatial and value distributions of the tensors issued from the dipolar splittings Monte Carlo simulations are represented as light gray point clouds in all figures.

prompted us to calculate the magnetic susceptibility tensor assuming a dimeric model for *R.C.* Cyt with the tensors derived from the dipolar shift studies.[19,20] Values are for the axial and rhombic anisotropies of 4.97×10^{-8} and 1.68×10^{-8} m^3/mol for spin state $S = 2$ and of 2.66×10^{-8} and 0.21×10^{-8} m^3/mol for spin state $S = {}^5/_2$. The corresponding Euler angles were −97.9°, 90°, and 180° for $S = 2$ and −16.5°, 90.0°, and 90.0° for spin state $S = {}^5/_2$. Figure 5 depicts the experimental $^1J_{NH}$ dipolar splittings and the $^1J_{NH}$ values simulated from the dipolar shift study assuming monomeric and dimeric models for both paramagnetic forms. The pattern of the experimental $^1J_{NH}$ clearly does not correspond to the simulated ones for the dimeric model. One can note that the correlations of the simulated data and the experimental data for the dimer model (see legends of Figure 5 and Figure S2 in Supporting Information) are fair, especially if one considers the spin state $S = 2$, but the amplitude effects are in much worse agreement. Correlation coefficients are in fact related to the orientation of the tensors whereas amplitude effects are determined by the amplitude of the anisotropy. The only dimeric model which would yield as good correlations with experimental data as the monomer model would be a molecule with a symmetry point instead of a symmetry axis. However, the simulated splittings with such a dimer model would be exactly twice those of the monomer model, and thus further incompatible with the experimental splittings.

To further characterize the oligomeric nature of cytochrome *c′*, we calculated the theoretical susceptibility tensor of spin state $S = 0$. Calculation assuming a monomeric protein yielded a tensor of anisotropies $\Delta\chi_{ax} = -0.94 \times 10^{-8}$ m^3/mol and $\Delta\chi_{rh} = 0.29 \times 10^{-8}$ m^3/mol characterized by the Euler angles (α,β,γ) = (72.6°, 132.9°, 91.0°) whereas assuming a dimeric molecule

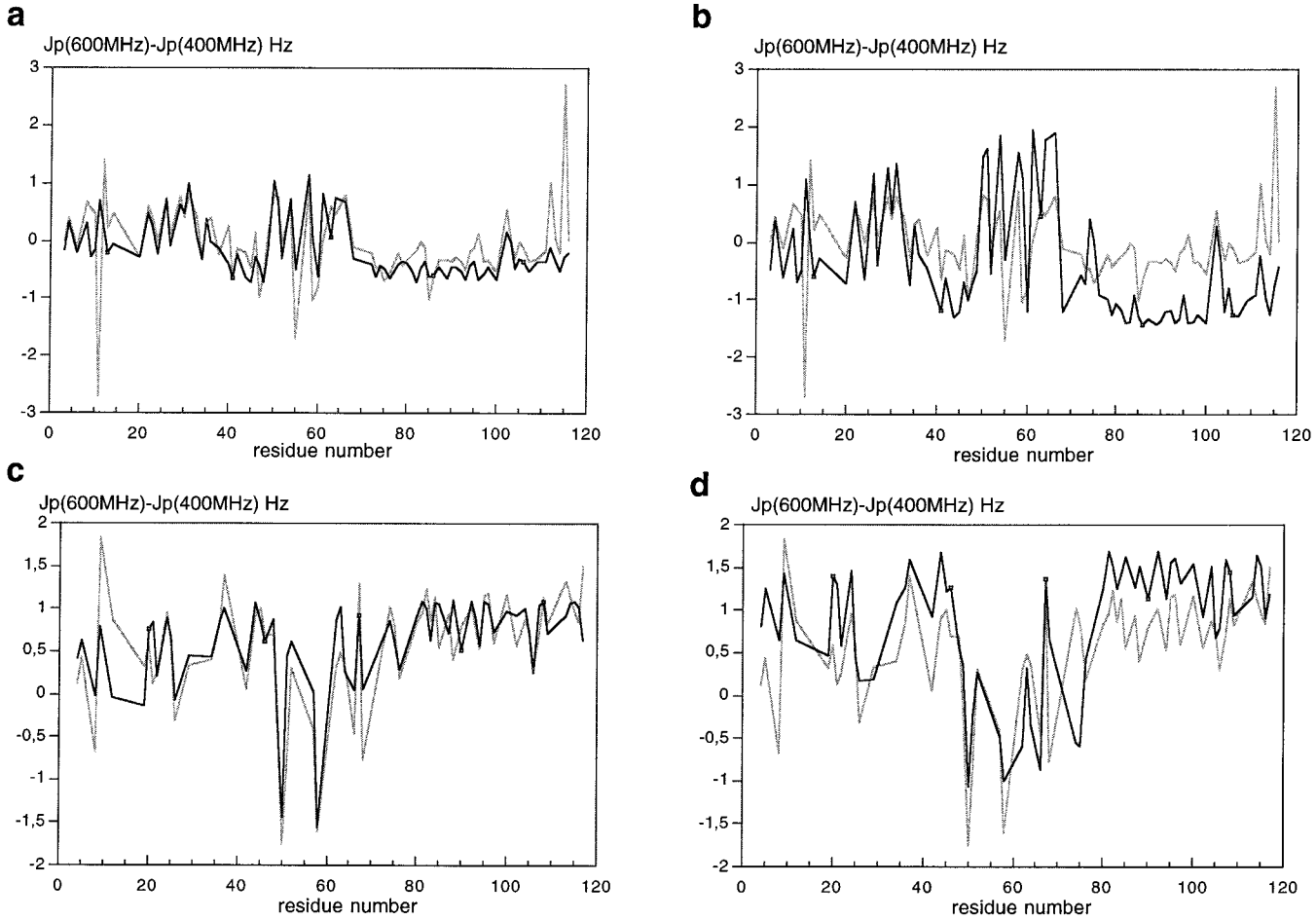

Figure 5. Plot of experimental dipolar splittings (light gray lines) and simulated dipolar splittings (black lines) for the reduced (a, b) and the oxidized (c, d) forms of the cytochrome *c′* of *Rb. capsulatus*. The experimental J^{dip} were taken as $J_{p(600MHz)} - J_{p(400MHz)}$. The calculated J^{dip} were obtained from eq 3 with $\chi = \chi_{cyt} + \chi_{dia}$, where χ_{dia} is the experiment derived susceptibility tensor for the diamagnetic form (Table 3, line C), χ_{cyt} is either the paramagnetic tensor χ_{dc} determined from the dipolar shift studies[19,20] (monomeric case) or the tensor resulting from the composition of the tensors of the two subunits (dimeric case).[45] The residue-specific order parameter *S* characterizing the orientational fluctuations of the NH bond was introduced as a scaling factor in eq 3. (a) For the paramagnetic form $S = 2$ assuming a monomeric molecule. (b) For the paramagnetic form $S = 2$, assuming a dimeric molecule. (c) For the paramagnetic form $S = {}^5/_2$, assuming a monomeric molecule. (d) For the paramagnetic form $S = {}^5/_2$, assuming a dimeric molecule. For reasons of clarity, the errors bars are not represented

yielded a tensor of anisotropies $\Delta\chi_{ax} = 1.38 \times 10^{-8}$ m^3/mol and $\Delta\chi_{rh} = 0.12 \times 10^{-8}$ m^3/mol characterized by the Euler angles $(\alpha,\beta,\gamma) = (-17.7°, 90.0°, 180.0°)$. Given the experiment-derived diamagnetic tensor (Table 2), the theoretical tensor for spin state $S = 0$ further supports the evidence that cytochrome *c′* is also monomeric when complexed with CO.

Structural Significance of the Monomer Model. The association state found for *R.C.* Cyt of strain M1131 in this study contrasts with data on other cytochromes *c′* and in particular with the cytochrome *c′* of *Rb. capsulatus* strain M110.[25] Although the fold of the monomeric subunit of M110-*R.C.* Cyt is very similar to other cytochromes *c′*, their relative organization in the dimer is unusual: they are almost parallel, in contrast to the X motif found in other bacteria.[25] The calculated association energy and interaction surface appear to be among the weakest found for cytochromes *c′*.[25] Interestingly, the replacement of the residue Glu90 by Asp90 in the M110 strain—a residue implicated in intermolecular contacts in the crystals but not belonging to the dimer interface—had dramatic consequences on the crystallization process and on the association state of the protein.[40] Crystallization of D90E *R.C.* Cyt from strain M110 occurs only in the presence of zinc ions and leads to monomeric species. These results suggest that the dimeric form of cytochrome *c′* of *Rb. capsulatus* may be energetically favored only in specific environments. This can account for the fact that former equilibrium sedimentation studies performed on *R.C.* Cyt yielded an apparent mass of 22.5 kD, an intermediate value between a monomer and a dimer form.[41] The sequence of strain M1131 moreover differs from that of strain M110 at position 38 by a Ala to Val mutation and this residue belongs to the dimer interface, establishing hydrophobic contact with the Ile46 of the second subunit.[42] Finally, it cannot be excluded that the dimeric state of M110-*R.C.* Cyt in the crystal is due to crystal packing effects. Work is currently in progress to determine if M110-*R.C.* Cyt is dimeric in solution. All the cytochromes *c′* whose structure have been solved by X-ray studies have been characterized as dimeric in the crystalline state but those of *Rhodobacter palustris*.[43] On the other hand, equilibrium sedimentation studies have determined a monomeric state for the cytochrome *c′* of *Rb. palustris* and a mixture of monomeric and dimeric states for the cytochrome *c′* of *Rhodobacter sphaeroides*.[41] The present study demonstrates that the functional state of *R.C.* Cyt is likely monomeric. These pieces of evidence suggest that the dimeric form of some cytochromes *c′* is not a strict requirement for their in vivo activity.

Use of Dipolar Splittings for Magnetism Characterization. The values of the principal components of the χ tensor in state $S = {}^5/_2$ and $S = 2$ either obtained from the dipolar shifts

measurements or derived from the residual dipolar splittings are similar. This has been already reported in the recent study of the paramagnetism of cytochrome b_5 where the tensor was derived from $^1J_{HN}$ splittings measured at 500 and 800 MHz on the paramagnetic form on one side and from a study of the dipolar shifts on the other side.[6] Determination of the zero-field splitting parameters from the principal component values affords an axial parameter D of -20.4 and -21.6 cm^{-1} and rhombic parameter $E = -3.3$ and -5 cm^{-1} for the $S = 2$ state and a D value of 10.6 and 10.1 cm^{-1} for the $S = {}^5/_2$ state using the one-field and two-field methods, respectively. These values are in very good agreement with those obtained from dipolar shifts (D -23.8 cm^{-1} and E -3 cm^{-1} for the $S = 2$ state, D 10.4 cm^{-1} for the $S = {}^5/_2$ state) or magnetic susceptibility measurements (D -18.3 cm^{-1} and E -3 cm^{-1} for the $S = 2$ state, D 12.3 cm^{-1} for the $S = {}^5/_2$ state).[19,20] Even if no diamagnetic reference is available, the determination of the residual dipolar splittings constitutes a powerful tool to study the magnetic behavior of metalloproteins. Indeed, in nonheminic proteins, the diamagnetic susceptibility only arises from the carbonyl bonds and side chains aromatic rings and its contribution to the χ tensor can be negligible. In this case, the two-field method gives directly a characterization of the paramagnetic susceptibility tensor as recently demonstrated for the iron center in a rubredoxin.[44] This method is thus very promising in particular for coupled systems as iron−sulfur cluster in ferredoxins, being the only way to determine the orientation of the tensor principal axis in these compounds at room temperature.

Conclusions

$^1J_{NH}$ splittings have been measured for the three magnetic states of *R.C.* Cyt at 600 and 400 MHz. The magnetic susceptibility tensor was characterized for the three forms using either data at one field or combining data at both fields. Both methods gave similar results. These magnetic susceptibility tensors are in good agreement with the data obtained from the paramagnetic chemical shifts, and the same deviation from the normal axis of the heme plane is observed from the $S = 2$ state. Comparison with the magnetic tensor derived from the dipolar shifts proved that the cytochrome *c*′ of *Rb. capsulatus* (strain M1131) is monomeric in the three states, opening the debate about the in vivo functionality of the association state of cytochrome *c*′. Dipolar splittings are thus useful tools either for determining the global fold of a protein or for characterizing the magnetic properties of paramagnetic centers in proteins. Moreover, information on the respective orientation of the subunits in a dimeric protein can be obtained from the comparison of the local and global magnetic tensors. There are a limited number of methods available to assess the oligomeric nature of a protein in the concentration range used for protein studies by NMR. NMR relaxation and diffusion investigations are the most used methods for this purpose. We show here that dipolar splitting measurements, even if not of use straightaway, can represent an alternative attractive way for the study of the oligomerization state of proteins.

Acknowledgment. The authors thank Dr. Bernhard Brutscher for critical reading of the manuscript, Dr. Martin Blackledge for helpful discussion, and Patrice Dosset for his programming help. Dr. M. Caffrey and Dr. M. Cusanovich are gratefully acknowledged for providing the protein cytochrome *c*′. This work was supported by the Commissariat à l'Energie Atomique, the CNRS and Molecular Simulations Inc. This is publication no. 719 of the Institut de Biologie Structurale "Jean-Pierre Ebel". H.D. was a recipient of a CEA postdoctoral fellowship.

Supporting Information Available: Six tables containing the splittings $^1J_{NH}$ determined for the three states of the cytochrome *c*′ of *Rb. capsulatus* at 400 MHz and 600 MHz. Figure S1 representing the experimental profiles of J^{dip} using the one-field method and the two-field method at 600 and 400 MHz for spin states $S = {}^5/_2$ and $S = 2$, with the error bars. Figure S2 representing the correlation plots of the experimental difference of dipolar splittings between 600 and 400 MHz versus the back-calculated ones from the dipolar shift derived magnetic tensor assuming either a monomeric model or a dimeric model.

References and Notes

(1) (a) Lohman, A. B.; MacLean, C. *Chem. Phys*. **1978**, *35*, 269−274. (b) Van Zijl, P. C. M.; Ruessing, B. K.; Bulthuis, J.; MacLean, C. *Acc. Chem. Res*. **1984**, *17*, 172−180. (c) Bastiaan, F. W.; Bulthuis, J.; MacLean, C. *Magn. Reson. Chem.* **1986**, *24*, 723−728.

(2) Tolman, J. R.; Flanagan, J. M.; Kennedy, M. A.; Prestegard, J. H. *Proc. Natl. Acad. Sci. U.S.A.* **1995**, *92*, 9279−9283.

(3) Tjandra, N.; Omichinski, J. G.; Gronenborn, A. M.; Clore, G. M.; Bax, A. *Nat. Struct. Biol*. **1997**, *4*, 732−738.

(4) (a) Tjandra, N.; Bax, A. *Science* **1997**, *278*, 1111−1114. (b) Prosser, R. S.; Losonczi, J. A.; Shiyanovskaya, I. V. *J. Am. Chem. Soc.* **1998**, *120*, 11010−11011. (c) Clore, G. M.; Starich, M. R.; Gronenborn, A. M. *J. Am. Chem. Soc.* **1998**, *129*, 10571−10572.

(5) Cai, M.; Huang, Y.; Zheng, R.; Wei, S. Q.; Ghirlando, R.; Lee, M. S.; Craigie, R.; Gronenborn, A. M.; Clore, G. M. *Nat. Struct. Biol.* **1998**, *5*, 903−909.

(6) Banci, L.; Bertini, I.; Huber, J. G.; Luchinat, C.; Rosato, A. *J. Am. Chem. Soc.* **1998**, *120*, 12903−12909.

(7) (a) Gochin, M.; Roder, H. *Protein Sci.* **1995**, *4*, 296−305. (b) Banci, L.; Bertini, I.; Gray, H. B.; Luchinat, C.; Redding, T.; Rosato, A.; Turano, P. *Biochemistry* **1997**, *36*, 9867−9877. (c) Banci, L.; Bertini, I.; Savellini, G. G.; Romagnoli, A.; Turano, P.; Cremonini, M. A.; Luchinat, C.; Gray, H. B. *Proteins* **1997**, *29*, 68−76. (d) Arnesano, F.; Banci, L.; Bertini, I.; Felli, I. C. *Biochemistry* **1998**, *37*, 173−189. (e) Banci, L.; Bertini, I.; De la Rosa, M. A.; Koulougliotis, D.; Navarro, J. A.; Walter, O. *Biochemistry* **1998**, *37*, 7, 4831−4843.

(8) Pettigrew, G. W.; Moore, G. R. *Cytochrome c*: *Biological aspects*; Springer-Verlag: Berlin, 1987.

(9) (a) Cusanovich, M. A.; Bartsch, R. G.; Kamen, M. D. *Biochim. Biophys. Acta* **1968**, *153*, 397−417. (b) Morita, S. *Biochim. Biophys. Acta* **1968**, *153*, 241−247.

(10) Bartsch, R. G. In *The Photosynthetic Bacteria*; Clayton, R. K., Sistrom, W. R., Eds.; Plenum: New York, 1978; pp 249−280.

(11) Yamanaka, T. *The Biochemistry of Bacterial Cytochromes*; Japan Scientific Societies Press: Tokyo, 1992; pp 89−168.

(12) Meyer, T.; Kamen, M. *Adv. Protein Chem.* **1982**, *35*, 105−212.

(13) Moore, G. R.; Pettigrew, G. W. *Cytochrome c*: *Evolutionary, Structural and Physicochemical Aspects*; Springer-Verlag: Berlin, 1990.

(14) Maltempo, M. M.; Moss, T. H. *Q. Rev. Biophys.* **1976**, *9*, 181−215.

(15) Bertini, I.; Gori, G.; Luchinat, C.; Vila, A. *Biochemistry* **1993**, *32*, 776−783.

(16) Emptage, M.; Xavier, A.; Wood, J.; Alsaadi, B.; Moore, G.; Pitt, R.; Williams, R.; Ambler, R.; Bartsch, R. *Biochemistry* **1981**, *20*, 58−64.

(17) (a) Moss, T. H.; Bearden, A. J.; Bartsch, R. G.; Cusanovich, M. A. *Biochemistry* **1968**, *7*, 1583−1590. (b) Emptage, M. H.; Zimmermann, R.; Que, L., Jr.; Münck, E.; Hamilton, W. D.; Orme-Johnson, W. H. *Biochim. Biophys. Acta* **1977**, *495*, 12−23.

(18) (a) Dutton, P. L.; Leigh, J. S. *Biochim. Biophys. Acta* **1973**, *314*, 178−190. (b) Prince, R. C.; Leigh, J. S.; Dutton, P. L. *Biochem. Soc. Trans*. **1974**, *314*, 178−190. (c) Corker, G. A.; Sharpe, S. A. *Photochem. Photobiol*. **1975**, *21*, 49−61. (d) Monkara, F.; Bingham, S. J.; Kadir, F. H. A.; McEwan, A. G.; Thomson, A. J.; Thurgood, A. G. P.; Moore, G. R. *Biochim. Biophys. Acta* **1992**, *1100*, 184−188.

(19) Tsan, P.; Caffrey, M.; Lawson, M.; Cusanovich, M. A.; Marion, D.; Gans, P., manuscript in preparation.

(20) Tsan, P.; Caffrey, M.; Lawson, M.; Cusanovich, M. A.; Marion, D.; Gans, P. *J. Am. Chem. Soc.* **1999**, *121*, 1795−1805.

(21) Caffrey, M.; Simorre, J. P.; Brutscher, B.; Cusanovich, M. A.; Marion, D. *Biochemistry* **1995**, *34*, 5904−5912.

(22) Tjandra, N.; Bax, A. *J. Magn. Reson.* **1997**, *124*, 512−515.

(23) Tjandra, N.; Grzesiek, S.; Bax, A. *J. Am. Chem. Soc*. **1996**, *118*, 6264−6272.

(24) Tolman, J. R.; Prestegard, J. H. *J. Magn. Reson. Ser. B* **1996**, *112*, 245−252.

(25) Tahirov, T. H.; Misaki, S.; Meyer, T. E.; Cusanovich, M. A.; Higuchi, Y.; Yasuoka, N. *J. Mol. Biol.* **1996**, *259*, 467−479.

(26) Blackledge, M. J.; Cordier, F.; Dosset, P.; Marion, D. *J. Am. Chem. Soc.* **1998**, *120*, 4538−4539.

(27) Kahn, O. *Molecular Magnetism*; VCH Publishers: New York, 1993.

(28) Bothner-By, A. A.; Gayathri, C.; van Zijl; P. C. M.; MacLean, J. J.; Smith, K. M. *Magn. Reson. Chem.* **1985**, *23*, 935−938.

(29) Giessner-Prettre, C.; Pullman, B. *Q. Rev. Biophys.* **1987**, *20*, 113−172.

(30) Williamson, M. P.; Asakura, T. J. *Magn. Reson. Ser. B* **1993**, *101*, 63−71. Tigelaar, H. L.; Flygare, W. H. *J. Am. Chem. Soc*. **1972**, *94*, 342−346.

(31) Harbison, G. S. *J. Am. Chem. Soc.* **1993**, *115*, 3026−3027.

(32) Ghose, R.; Prestegard, J. H. *J. Magn. Reson*. **1997**, *128*, 138−143.

(33) Assuming a correlation time of 10 ns, and using the formula given by Tjandra et al.:[23] $^1J_{\mathrm{NHdiaDFS}} = 1/(20\pi^3)h\Delta\sigma\gamma_{\mathrm{N}}\gamma_{\mathrm{H}}(r_{\mathrm{NH}})^{-3}[1 + (\gamma_{\mathrm{N}}B\tau_{\mathrm{c}})^{-2}]^{-1}$.

(34) Golding, R.; Pascual, R.; Stubbs, L. *Mol. Phys.* **1976**, *106*, 7170−7177.

(35) From the measure of the axial and rhombic anisotropies, one can derive the three parameters χ_x, χ_y, and χ_z by postulating that the trace of the χ tensor is equal to zero. It is straightforward to verify that the axial and rhombic anisotropies of the equivalent minima are independent of the trace value.

(36) Bougault, C. M.; Dou, Y.; Ikeda-Saito, M.; Langry, K. C.; Smith, K. M.; La Mar, G. N. *J. Am. Chem. Soc.* **1998**, *120*, 2113-2123.

(37) Cordier, F.; Caffrey, M.; Brutscher, B.; Cusanovich, M. A.; Marion, D.; Blackledge, M. J. *J. Mol. Biol.* **1998**, *281*, 341−361.

(38) Lipari, G.; Szabo, *A. J. Am. Chem. Soc.* **1982**, *104*, 4546−4559.

(39) Tsan, P.; Hus, J. C.; Caffrey, M.; Marion, D.; Blackledge, M.**,** submitted for publication.

(40) Tahirov, T. H.; Mikasi, S.; Meyer, T. E.; Cusanovich, M. A.; Higuchi, Y.; Yasuoka, N. *Acta Crystallogr.* **1997**, *D53*, 658−664.

(41) Cusanovich, M. A. *Biochim. Biophys. Acta* **1970**, *236*, 238−241.

(42) Tsan, P. Doctorat d'Université, Université Joseph Fourier, Grenoble, France, 1998.

(43) Shibata, N.; Iba, S.; Misaki, S.; Meyer, T. E.; Bartsch, R. G.; Cusanovich, M. A.; Morimoto, Y.; Higuchi, Y.; Yasuoka, N. *J. Mol. Biol.* **1998**, *284*, 751−760.

(44) Volkman, B. F.; Wilkens, S. J.; Lee, A. L.; Xia, B.; Westler, W. M.; Beger, R.; Markley, J. L. *J. Am. Chem. Soc.* **1999**, *121*, 4677−4683.

(45) The tensor for a dimeric molecule composed of two subunits A and B related by an axis symmetry **s** can be calculated from the subunit A tensor by: $\chi_{\mathrm{dim}} = \chi_{\mathrm{A}} + \boldsymbol{s}\chi_A\,\mathbf{s}$. In the symmetry frame, the symmetry operator around the *z* axis $\mathbf{s_{Oz}}$ is expressed by

$$\begin{bmatrix} -1 & 0 & 0 \\ 0 & -1 & 0 \\ 0 & 0 & 1 \end{bmatrix}$$